Journal of Power Sources 189 (2009) 139–144

Contents lists available at ScienceDirect

Journal of Power Sources

journal homepage: www.elsevier.com/locate/jpowsour

Self-supported poly(methyl methacrylate–acrylonitrile–vinyl acetate)-based gel electrolyte for lithium ion battery

Y.H. Liao [a], D.Y. Zhou [a], M.M. Rao [a], W.S. Li [a,b,*], Z.P. Cai [a], Y. Liang [a], C.L. Tan [a,b]

[a] School of Chemistry and Environment, South China Normal University, Guangzhou 510006, China
[b] Key Lab of Electrochemical Technology on Energy Storage and Power Generation in Guangdong Universities, Guangzhou 510006, China

ARTICLE INFO

Article history:
Received 2 July 2008
Received in revised form 1 September 2008
Accepted 5 October 2008
Available online 17 October 2008

Keywords:
P(MMA–AN–VAc)
Gel polymer electrolyte
Stability
Conductivity
Lithium ion battery
Self-supported

ABSTRACT

Self-supported gel polymer electrolyte (GPE) was prepared based on copolymer, poly(methyl methacrylate–acrylonitrile–vinyl acetate) (P(MMA–AN–VAc)). The copolymer P(MMA–AN–VAc) was synthesized by emulsion polymerization and the copolymer membrane was prepared through phase inversion. The structure and the performance of the copolymer, the membrane and the GPE were characterized by FTIR, NMR, SEM, XRD, DSC/TG, LSV, CA, and EIS. It is found that the copolymer was formed through the breaking of double bond C=C in each monomer. The membrane has low crystallinity and has low glass transition temperature, 39.1 °C, its thermal stability is as high as 310 °C, and its mechanical strength is improved compared with P(MMA–AN). The GPE is electrochemically stable up to 5.6 V (vs. Li/Li$^+$) and its conductivity is 3.48×10^{-3} S cm^{-1} at ambient temperature. The lithium ion transference number in the GPE is 0.51 and the conductivity model of the GPE is found to obey the Vogel–Tamman–Fulcher (VTF) equation.

1. Introduction

Among the commercial rechargeable batteries, lithium ion battery has highest energy density, thus finds its wider application than any other rechargeable battery. However, lithium ion battery faces serious safety problem, which results from the use of liquid electrolyte containing flammable organic solvents. This problem can be solved by using solid polymer electrolyte (SPE) without any solvent molecules. But the low ionic conductivity of SPE, about 1×10^{-5} S cm^{-1} at room temperature, which is three decades lower than that of the conventional liquid electrolyte, is not suitable for the lithium ion battery use. Gel polymer electrolyte (GPE), which uses polymer as a matrix to convert liquid organic solvents into gel, is an alternative to SPE for solving the safety problem of lithium ion battery [1,2]. So far, many polymers have been reported to be used as matrixes for GPE, such as poly(vinylidenefluoride) (PVDF) [3,4], polyacrylonitrile (PAN) [5], poly(methyl methacrylate) (PMMA) [6], poly(ethylene oxide) (PEO) [7], polyvinyl chloride (PVC) [8]. However, the GPEs based on these matrixes are formed by the same monomers, thus lack good comprehensive performance. For example, mechanical strength is good but ionic conductivity is poor and vice versa.

The poor comprehensive performance of the GPE with monopolymer as matrix can be improved to different extents by using copolymers from monomers with different functions. For example, the performance of the GPE with PMMA or PAN as matrix can be improved by using the copolymer of MMA and AN [9–12]. This paper develops a new copolymer, poly(methyl methacrylate–acrylonitrile–vinyl acetate) (P(MMA–AN–VAc)), to obtain a GPE with good comprehensive performance by employing the individual advantages of MMA, AN and vinyl acetate (VAc). AN provides the copolymer with good processability, electrochemical and thermal stability [13]. MMA provides the copolymer with good electrolyte uptake and reduce the brittleness of the copolymer due to the use of AN [14–16]. VAc provides the GPE with strong adhesion to the anode or cathode materials and excellent mechanical stability [17]. Compared with P(MMA–AN)-based GPE, P(MMA–AN–VAc)-based GPE has higher ionic conductivity, better mechanical strength, electrochemical and thermal stability.

2. Experimental

2.1. Preparation

Commercial MMA (>99.5%), AN (>99.5%) and VAc (>99.5%) were distilled in vacuum to remove the aggregation inhibitor. The

* Corresponding author at: School of Chemistry and Environment, South China Normal University, Guangzhou 510006, China. Tel.: +86 20 39310256; fax: +86 20 39310256.
E-mail address: liwsh@scnu.edu.cn (W.S. Li).

0378-7753/$ – see front matter © 2008 Elsevier B.V. All rights reserved.
doi:10.1016/j.jpowsour.2008.10.027

monomers, MMA, AN and VAc, were mixed in mole ratio of 1:2:1. The used ratio of MMA to AN in this work was based on our previous results for P(MMA–AN) preparation [2]. Sodium dodecyl sulfate (SDS) as an emulsifier was dissolved in the deionized water with a concentration of 1.5 wt% to form a homogeneous emulsion solution under N_2 flow at 60 °C, then the monomer mixture was added into emulsion solution under stirring vigorously (1000 rpm) for 6 h. During the reaction, 0.15 wt% sodium persulfate (NaPS) as an initiator was added into the emulsion solution in two batches. The resulting solution was poured into 3 wt% Al_2SO_4 solution to yield the precipitate, which was isolated by filtration and washed with the hot deionized water and ethanol successively for the removal of any impurities such as residual monomers and emulsifier. The product of white powder was obtained by drying the cleaned precipitate in a vacuum oven at 60 °C for 24 h and kept in a desiccator for membrane preparation.

The prepared P(MMA–AN–VAc) copolymer was dissolved at a concentration of 7 wt% in dimethylformamide (DMF) at 80 °C for 30 min. After complete dissolution, the resulting viscous solution was cast with a doctor blade onto a glass plate, inducing phase inversion. The resulting membrane was washed with running water, immersed in deionized water for 2 h, dried in vacuum at 60 °C for 24 h and finally porous membrane was obtained.

In order to obtain GPE, the porous membrane was immersed in an electrolyte solution, 1 M $LiPF_6$ in ethylene carbonate (EC)/dimethyl carbonate (DMC)/diethyl carbonate (DEC) (1:1:1 in mass) for 30 min in an argon-filled glove box (Mikrouna).

2.2. Characterization

The structure of the copolymer was characterized by Fourier transform infrared (FTIR) (Perkin Elmer Spectrograph) in the range of 450–4000 cm^{-1}, nuclear magnetic resonance (NMR) (Varian 400 Spectrometer, USA) employing dimethyl sulphoxide (DMSO) as the solvent at 60 °C and X-ray diffraction (XRD) (Rigaku D/MAX-RC, Japan) in the degree range from 5° to 90°. The morphology of the polymer membrane was characterized by scanning electron microscopy (SEM) (JEOL, JSM-6380LV, Japan) at an acceleration voltage of 15 kV. The differential scanning calorimetry (DSC) traces and the thermogravimetric analysis (TGA) were obtained using a Netzsch DSC 200-PC and Netzsch STA-409PC analyser instrument to survey the glass transition temperature and thermal stability of the membrane. Mechanical strength of the membrane was measured on Gotech GT-TS-2000.

The electrochemical stability of the GPE was determined on the electrochemical instrument (CHI650B, Shanghai) by the linear sweep voltammetry (LSV) with the cell Li/GPE/stainless steel (SS). The SS was used as working electrode and the lithium as the reference and the counter electrodes. The potential scanning rate is 1 mV s^{-1}. The lithium ion transference number was measured by the combination of chronoamperometry (CA) and electrochemical impedance spectroscopy (EIS) using a symmetrical cell Li/GPE/Li. The ionic conductivity of the GPE was measured with a cell SS/GPE/SS by EIS with ac amplitude of 10 mV from 100 kHz to 1 Hz.

3. Results and discussion

3.1. FTIR spectrum

Fig. 1 presents the FTIR spectra of monomers, MMA, AN and VAc, and their copolymer, P(MMA–AN–VAc). The characteristic adsorption peaks of MMA are at 1638 cm^{-1} for the bond C=C and 1729 cm^{-1} for the stretching bond C=O [18,19]. The AN is characteristic of the adsorption peaks at 1619 and 2239 cm^{-1}, which corresponds to the bonds C=C and C≡N, respectively [2,12]. The VAc shows its characteristic absorption at 1648 and 1761 cm^{-1}, which corresponds to the bonds C=C and C=O, respectively [20]. Comparing the FTIR spectrum of the copolymer with those of monomers, it can be seen that the copolymer still keeps the absorptions at 1730 cm^{-1} (bond C=O) and 2242 cm^{-1} (bond C≡N), but loses the absorption at 1638, 1619 or 1648 cm^{-1} for each monomer's C=C groups. This indicates the copolymer is obtained by the way of the breaking each monomer's double bonds C=C, while maintains the main characteristics of the monomers, as shown in Scheme 1. Based on the molecular weight of P(MMA–VAc), 1.26 million, which was prepared under the similar conditions [1], it can be inferred that the molecular weight of the P(MMA–AN–VAc) should be over 1 million.

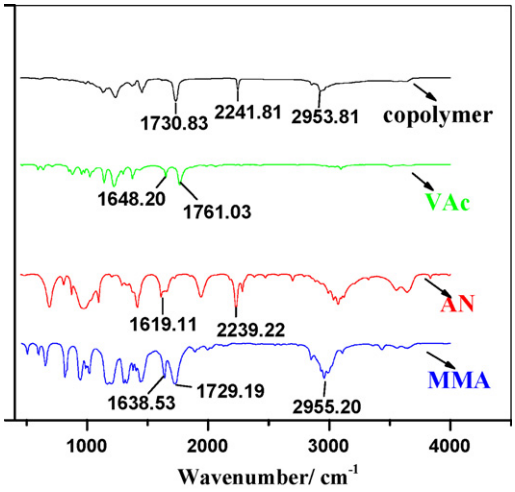

Fig. 1. FTIR spectra of monomers, MMA, AN and VAc, and their copolymer.

3.2. NMR spectrum

Fig. 2 presents the ^1H NMR and ^{13}C NMR spectra of the copolymer. Fig. 2a shows α-methyl protons (CH_3) and the methylene protons (CH_2) on main chain of copolymer at the range of around 1.0–1.4δ and 1.8–2.2δ, respectively. The peak at 2.5δ is caused by the proton of DMSO solvent. The peaks at 2.8–3.2δ are ascribed to the proton peaks of methine carbon (CH) on main chain which is connected with cyanate carbon (C≡N) in copolymer. The peak for methoxy protons (O–CH_3) connected with adjacent carbonyl group in the MMA unit is at 3.4δ. The peak at around 3.6δ is due to the methine protons (O–CH) connected with carbonyl carbon on main chain of copolymer, which is corresponding to the VAc chain [21,22].

Fig. 2b shows the methylene carbon (CH_2) at 27–29δ, the methine carbon (CH) at 33–34δ, and cyanate carbon (CN) at 120–121δ [24]. This is matched with the typical carbon of P(MMA–AN–VAc) and is in agreement with the results obtained from FTIR spectra. The mole ratio of MMA, AN and VAc units in P(MMA–AN–VAc), obtained from hydrogen atom number calculation, is 0.9:1.9:1. This is in accord with the monomer ratio of starting materials.

3.3. SEM image

Fig. 3 presents the SEM images of the P(MMA–AN–VAc) membrane before and after the immersion in liquid electrolyte. In the phase inversion process, the porous membrane is formed by exchange between solvent (DMF) and non-solvent (water). It can be seen from Fig. 3a that the self-supported membrane has a large

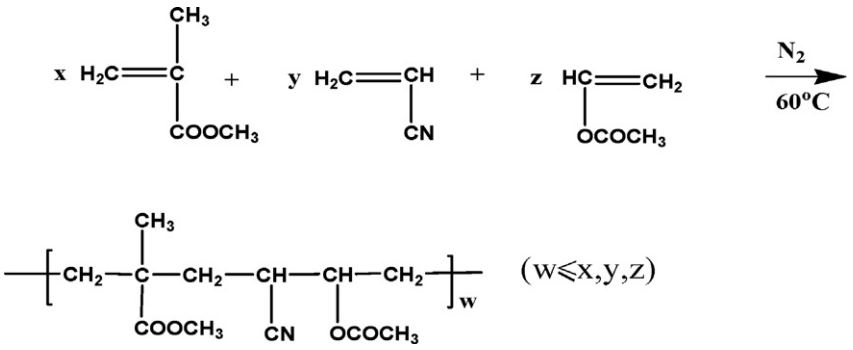

Scheme 1. Synthesis route of P(MMA–AN–VAc) copolymer prepared by emulsion polymerization.

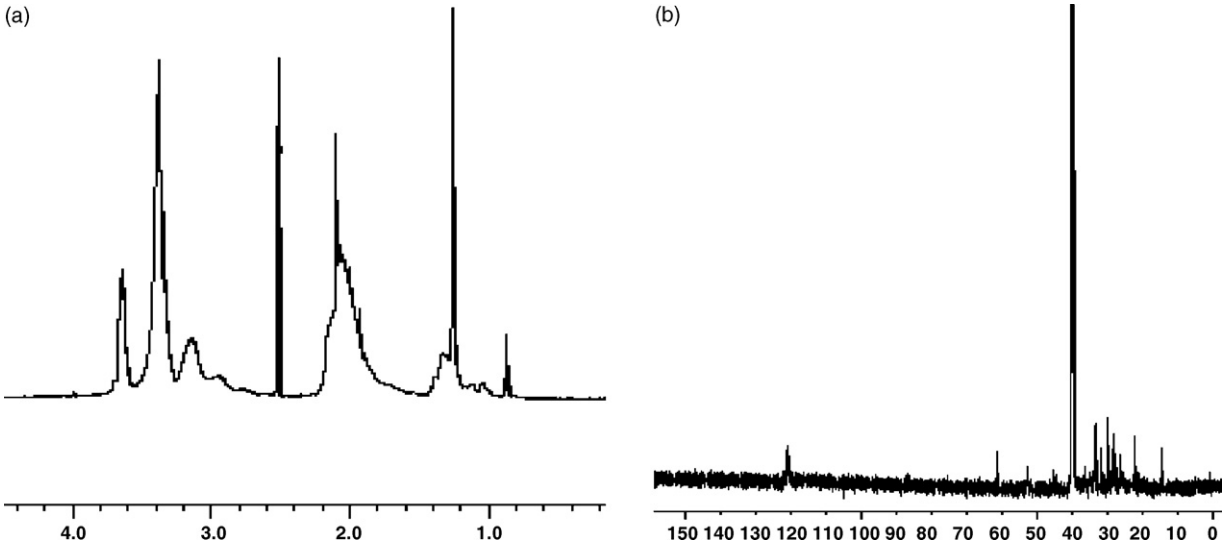

Fig. 2. ^{1}H NMR spectrum (a) and ^{13}C NMR spectrum (b) in P(MMA–AN–VAc).

number of pores with an average diameter of 0.5 μm on the surface and plenty of interconnected pores under the surface, which are necessary for a membrane to have high ionic conductivity. Fig. 3b shows the SEM image of the dried P(MMA–AN–VAc) membrane after immersion in electrolyte (1 M $LiPF_6$ in EC/DMC/DEC (1:1:1 in mass)). The mass of the dried membrane after immersion is almost equal to that of the membrane before immersion. It can be seen from Fig. 3b that the membrane almost keeps its interconnected pore structure after the immersion. This indicates that the membrane is stable chemically when it absorbs the liquid electrolyte.

3.4. XRD pattern

Fig. 4 shows the XRD patterns of PMMA, P(MMA–AN) and P(MMA–AN–VAc). In Fig. 4a, one relatively strong diffraction peak is found at $2\theta = 12.9^{\circ}$ for PMMA, which reflects the crystallization

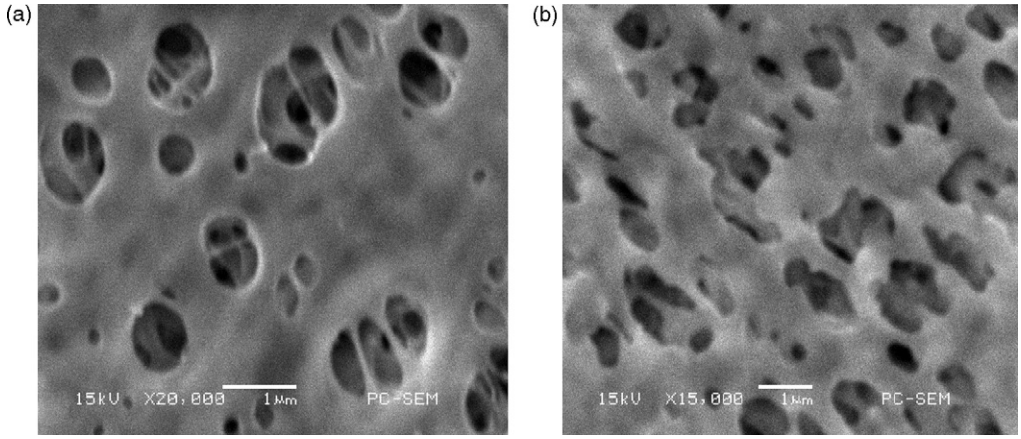

Fig. 3. SEM images of dry P(MMA–AN–VAc) membrane before (a) and after (b) immersion in liquid electrolyte.

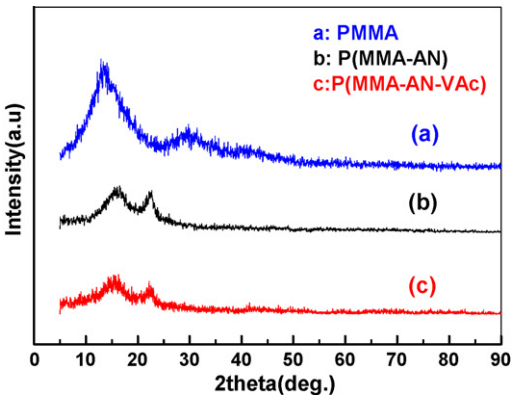

Fig. 4. X-ray diffraction patterns of PMMA (a), P(MMA–AN) (b) and P(MMA–AN–VAc) (c).

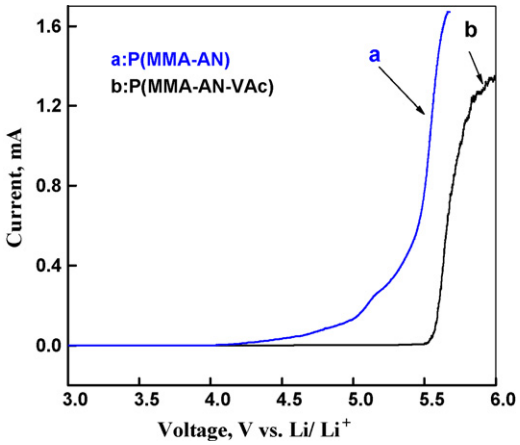

Fig. 6. Linear sweep voltammograms on stainless steel for GPE with P(MMA–AN) (a) and P(MMA–AN–VAc) (b) as matrixes, scanning rate: 1 mV s^{-1}.

of polymer [23]. P(MMA–AN) also has diffraction peaks, indicating that P(MMA–AN) is characteristic of crystallization, as shown in Fig. 4b. This result is consistent with that reported by Shi et al. [24]. P(MMA–AN–VAc) has the similar diffraction with P(MMA–AN), as shown in Fig. 4c. It can be found by comparing Fig. 4b and Fig. 4c that the diffraction peaks of P(MMA–AN–VAc) are broader and weaker than those of P(MMA–AN), indicating that P(MMA–AN–VAc) has lower crystallinity than P(MMA–AN). Based on the calculation using the MDI Jade 5.0 program, the crystallinity of P(MMA–AN) and P(MMA–AN–VAC) is 29.02% and 11.04%, respectively. PVAc is amorphous [25], thus the addition of the monomer VAc to P(MMA–AN) may reduce the crystallinity and increase the amorphous nature of the copolymer, leading to reduce the energy barrier to the chain movement [25]. Therefore, the lower crystallinity of the P(MMA–AN–VAc) is expected to contribute high ionic conductivity to the P(MMA–AN–VAc)-based GPE.

3.5. Thermal stability

Fig. 5a presents the DSC curve of P(MMA–AN–VAc) copolymer membrane from −50 to 80 °C. The glass transition temperature (T_g) of the copolymer is only 39.1 °C, much lower than that of pure PAN (about 90 °C) [26,27], PMMA (113 °C) [28], or P(MMA–AN) (98 °C) [29]. This confirms that the copolymer is formed by the copolymerization among three monomers rather than the co-mixture of PAN, PMMA and PVAc. The lower T_g of the copolymer weakens the interaction between the ionic liquid electrolyte and copolymer matrix, which will help the segmental motion and thus increase the ionic conductivity of the GPE.

The thermal stability of the copolymer was determined by TGA under N_2 atmosphere from room temperature to 700 °C at a heating rate of 10 °C min^{-1}. The obtained result is shown in Fig. 5b. It can be seen from Fig. 5b that the copolymer is stable up to 310 °C. This indicates that P(MMA–AN–VAc) has better thermal stability than P(MMA–AN), whose thermal stability is lower than 300 °C [2,12].

3.6. Mechanical strength

The mechanical strength of the P(MMA–AN–VAc) membrane was determined at a crosshead speed of 10 mm min^{-1} at room temperature. The obtained fracture strength of the membrane is 8.21 MPa, which is far higher than that of the P(MMA–AN) membrane (4.88 MPa) [29]. This phenomenon can be interpreted by the addition of VAc monomer which has excellent mechanical stability [17].

3.7. Electrochemical stability

Fig. 6 presents linear sweep voltammograms of P(MMA–AN–VAc)- and P(MMA–AN)-based gel electrolyte, obtained from the cell SS/GPE/Li. It can be seen from the curve (a) of Fig. 6 that the P(MMA–AN)-based gel electrolyte decomposes at about 4.5 V (vs. Li/Li^+). However, the P(MMA–AN–VAc)-based gel electrolyte is stable up to 5.6 V (vs. Li/Li^+), as seen from the curve (b) of Fig. 6. This indicates that P(MMA–AN–VAc)-based gel electrolyte

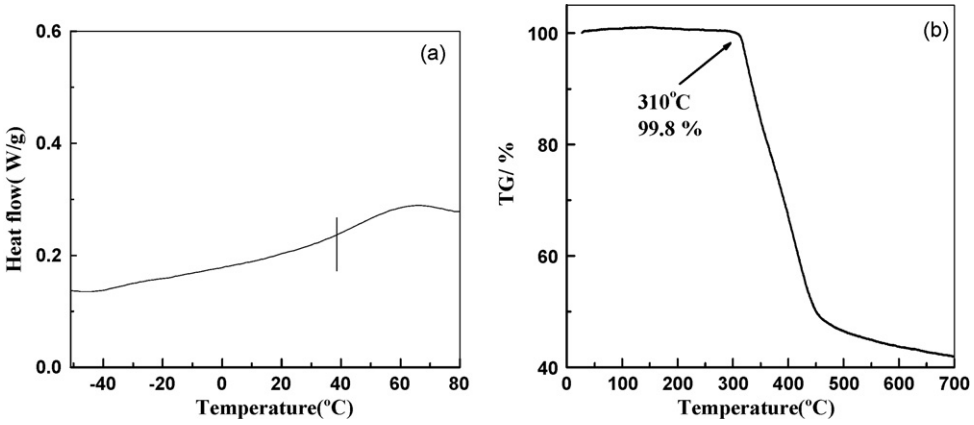

Fig. 5. DSC (a) and TG (b) curves of P(MMA–AN–VAc) membrane.

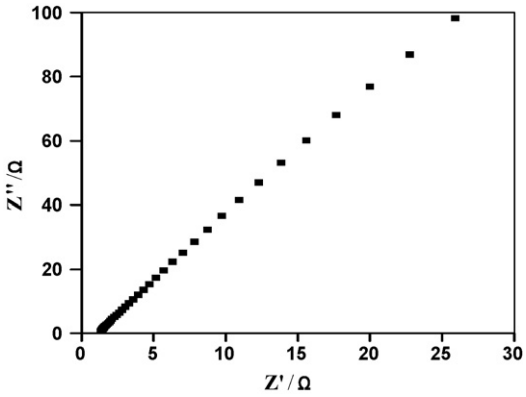

Fig. 7. The Nyquist plot of the cell SS/P(MMA–AN–VAc)-based GPE/SS at room temperature.

has better electrochemical stability than P(MMA–AN)-based gel electrolyte.

3.8. Lithium ion transference number

The lithium ion transference number (t_+) in GPE is one of the most important parameters that affect the performance of lithium ion battery. It can be obtained by CA and EIS according to the following equation [30]:

$$t_+ = \frac{I_S(\Delta V - I_0 R_0)}{I_0(\Delta V - I_S R_S)} \quad (1)$$

where ΔV is the potential applied to the cell in CA, I_0 the initial current, I_S the steady-state current, R_0 the charge transfer resistance before the polarization, and R_S is the steady-state charge transfer resistance after the polarization. The charge transfer resistances were determined by EIS. The ideal value of t_+ is one, since the t_+ lower than one would tend to develop concentration gradients at electrode surfaces and leading to limiting currents [31]. In fact, the oxygen and nitrogen atoms of solvent molecules in electrolyte always coordinate with lithium ions and anion ions in electrolyte afforded a fraction of conductivity, the t_+ in electrolyte is far lower than one. In GPE, the t_+ is about 0.5.

In this work, the used ΔV is 10 mV, the measured I_0 and I_S were 2.85 and 1.52 μA, and the measured R_0 and R_S were 341 and 381 Ω, respectively. The obtained t_+ from Eq. (1) is 0.51, which is slightly higher than that of PMMA-blend system [32] or PVdF–HFP system [33]. The higher transference number can help to decrease concentration polarization in the inner battery, thus the battery can work under high current density [34,35].

3.9. Ionic conductivity

In order to determine the ionic conductivity, GPE was sandwiched between two parallel SS discs (diameter Φ = 16 mm). The ionic conductivity (σ) was calculated from the bulk electrolyte resistance (R) according to the following equation:

$$\sigma = \frac{l}{RS} \quad (2)$$

where l is the thickness of GPE, and S is the contact area between GPE and SS disc. The bulk electrolyte resistance R was obtained by EIS.

Fig. 7 presents the Nyquist plot of the GPE with P(MMA–AN–VAc) as matrix at room temperature. It can be seen that the imaginary part of the impedance is linearly related to its real part. The intersection of the straight line with the real part axis is the bulk electrolyte resistance (R). The ionic conductivity of the GPE calculated from Eq. (2) is 3.48×10^{-3} S cm^{-1} at room temperature, which is higher than that of the GPE with P(AN–MMA) as matrix [10,12].

The high ionic conductivity of the P(MMA–AN–VAc)-based GPE should be ascribed to the interconnected pores in P(MMA–AN–VAc) membrane, the high lithium ion transference number and the increase in amorphous phase. Unlike other GPE, in which the increase in ionic conductivity is usually at the cost of chemical and mechanical stability, the P(MMA–AN–VAc)-based GPE has not only high ionic conductivity but also high chemical and mechanical stability.

To further understand the conductivity mechanism of P(MMA–AN–VAc)-based GPE, the ionic conductivity of the GPE was determined under different temperatures. The absolute temperature dependence of the ionic conductivity of P(MMA–AN–VAc)-based GPE is shown in Fig. 8. The ionic conductivity increases with the absolute temperature, but it is not related to the absolute temperature in a linear relationship, as shown in Fig. 8a. This suggests that the conductivity of P(MMA–AN–VAc)-based GPE does not obey the Arrhenius law. On the other hand, the experimental result can be well fitted by the Vogel–Tamman–Fulcher (VTF) equation, as shown in Fig. 8b. This behavior is characteristic of the amorphous polymeric electrolytes [36], which follows free-volume model [37,38]. The

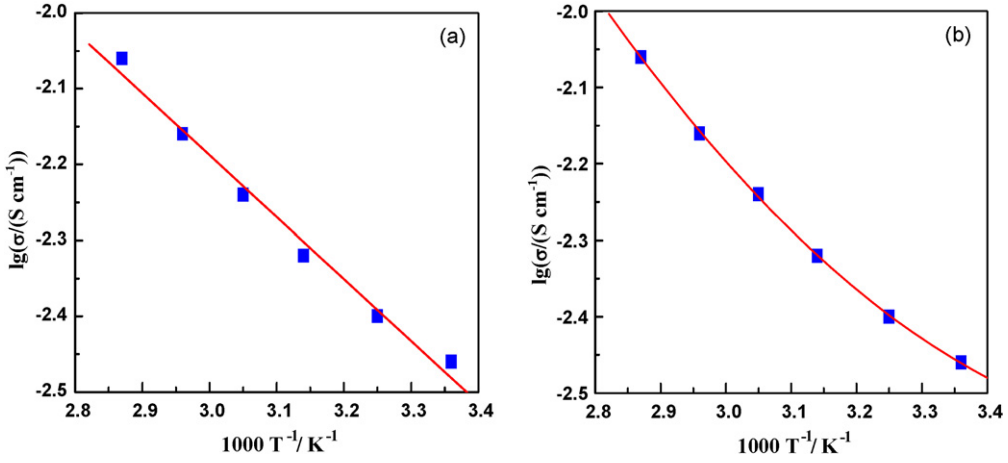

Fig. 8. Temperature dependence of ionic conductivity of P(MMA–AN–VAc)-based GPE, dot: experimental; line: fitted results with Arrhenius equation (a) and VTF equation (b).

Vogel–Tamman–Fulcher (VTF) equation is [39]:

$$\sigma = AT^{-1/2} \exp\left[-\frac{B}{T - T_0}\right] \quad (3)$$

where A and B are the constants related to the number of charge carriers and the activation energy for ion conduction, respectively, T_0 is the reference temperature and usually approximate to the glass transition temperature T_g. T_0 obtained from fitting is 313.38 K (40.23 °C). This is close to the T_g obtained by the DSC measurement.

4. Conclusion

A new gel polymer electrolyte, based on self-supported P(MMA–AN–VAc), was developed in this paper. The developed GPE has high ionic conductivity as well as high electrochemical, thermal and mechanical stability. The high ionic conductivity can be ascribed to the low crystallinity of the P(MMA–AN–VAc) and interconnected porous structure of the P(MMA–AN–VAc) membrane.

References

[1] L. Lu, X.X. Zuo, W.S. Li, J.S. Liu, M.Q. Xu, Acta Chim. Sinica 65 (2007) 475–480.
[2] M.M. Rao, J.S. Liu, W.S. Li, Y. Liang, D.Y. Zhou, J. Membr. Sci. 322 (2008) 314–319.
[3] Z.H. Li, P. Zhang, H.P. Zhang, Y.P. Wu, X.D. Zhou, Electrochem. Commun. 10 (2008) 791–794.
[4] X.X. Zuo, M.Q. Xu, W.S. Li, D.G. Su, J.S. Liu, Electrochem. Solid-State Lett. 9 (2006) A196–A199.
[5] F. Yuan, H.Z. Chen, H.Y. Yang, H.Y. Li, M. Wang, Mater. Chem. Phys. 89 (2005) 390–394.
[6] J.D. Jeon, B.W. Cho, S.Y. Kwak, J. Power Sources 143 (2005) 219–226.
[7] H. Cheng, C.B. Zhu, B. Huang, M. Lu, Y. Yang, Electrochim. Acta 52 (2007) 5789–5794.
[8] S. Rajendran, M.R. Prabhu, M.U. Rani, J. Power Sources 180 (2008) 880–883.
[9] S.S. Zhang, M.H. Ervin, K. Xu, T.R. Jow, Electrochim. Acta 49 (2004) 3339–3345.
[10] W.H. Pu, X.M. He, L. Wang, Z. Tian, C.Y. Jiang, C.R. Wan, J. Membr. Sci. 280 (2006) 6–9.
[11] P. Zhang, H.P. Zhang, G.C. Li, Z.H. Li, Y.P. Wu, Electrochem. Commun. 10 (2008) 1052–1055.
[12] D.Y. Zhou, G.Z. Wang, W.S. Li, G.L. Li, C.L. Tan, M.M. Rao, Y.H. Liao, J. Power Sources 184 (2008) 477–480.
[13] G. Wu, H.Y. Yang, H.Z. Chen, F. Yuan, L.G. Yang, M. Wang, R.J. Fu, Mater. Chem. Phys. 104 (2007) 284–287.
[14] K.H. Lee, Y.G. Lee, J.K. Park, D.Y. Seung, Solid State Ionics 133 (2000) 257–263.
[15] S.S. Zhang, K. Xu, T.R. Jow, Solid State Ionics 158 (2003) 375–380.
[16] S.S. Zhang, T.R. Jow, J. Power Sources 109 (2002) 422–426.
[17] R. Baskaran, S. Selvasekarapandian, N. Kuwata, J. Kawamura, T. Hattori, J. Phys. Chem. Solids 68 (2007) 407–412.
[18] S. Rajendran, M. Sivakumar, R. Subadevi, J. Power Sources 124 (2003)225–230.
[19] S.P. Zhang, X.K. Fu, Y.F. Gong, J. Appl. Polym. Sci. 106 (2007) 4091–4097.
[20] R. Baskaran, S. Selvasekarapandian, G. Hirankumar, M.S. Bhuvaneswari, J. Power Sources 134 (2004) 235–240.
[21] Z.L. Wang, Z.Y. Tang, Electrochim. Acta 49 (2004) 1063–1068.
[22] W.H. Pu, X.M. He, L. Wang, Z. Tian, C.Y. Jiang, C.R. Wan, Ionics 14 (2008) 27–31.
[23] H.P. Zhang, P. Zhang, Z.H. Li, M. Sun, Y.P. Wu, H.Q. Wu, Electrochem. Commun. 9 (2007) 1700–1703.
[24] S. Shi, S. Kuroda, K. Hosoi, H. Kubota, Polymer 46 (2005) 3567–3570.
[25] R. Baskaran, S. Selvasekarapandian, N. Kuwata, J. Kawamura, T. Hattori, Solid State Ionics 177 (2006) 2679–2682.
[26] Y.H. Liang, C.C. Wang, C.Y. Chen, J. Power Sources 176 (2008) 340–346.
[27] P.A.R.D. Jayathilaka, M.A.K.L. Dissanayake, I. Albinsson, B.E. Mellander, Solid State Ionics 156 (2003) 179–195.
[28] D.W. Kang, D.W. Kim, S.I. Jo, H.J. Sohn, J. Power Sources 112 (2002) 1–7.
[29] Z. Tian, X.M. He, W.H. Pu, C.R. Wan, C.Y. Jiang, Electrochim. Acta 52 (2006) 688–693.
[30] P.G. Bruce, C.A. Vincent, J. Electroanal. Chem. 225 (1987) 1–17.
[31] F.B. Dias, L. Plomp, J.B.J. Veldhuis, J. Power Sources 88 (2000) 169–191.
[32] D. Shanmukaraj, G.X. Wang, R. Murugan, H.K. Liu, J. Phys. Chem. Solids 69 (2008) 243–248.
[33] M. Stolarska, L. Niedzicki, R. Borkowska, A. Zalewska, W. Wieczorek, Electrochim. Acta 53 (2007) 1512–1517.
[34] K.L. Heitner, J. Power Sources 89 (2000) 128–131.
[35] J.M. Tarascon, M. Armand, Nature 414 (2001) 359.
[36] A.M. Christie, L. Christie, C.A. Vincent, J. Power Sources 74 (1998) 77–86.
[37] S. Ahmad, T.K. Saxena, S. Ahmad, S.A. Agnihotry, J. Power Sources 159 (2006) 205–209.
[38] A.M.M. Ali, N.S. Mohamed, A.K. Arof, J. Power Sources 74 (1998) 135–141.
[39] F.A. Amaral, C. Dalmolin, S.C. Canobre, N. Bocchi, R.C. Rocha-Filho, S.R. Biaggio, J. Power Sources 164 (2007) 379–385.